Journal of Materials and Environmental Science
ISSN : 2028-2508
CODEN : JMESCN

J. Mater. Environ. Sci., 2020, Volume 11, Issue 9, Page 1512-1530

http://www.jmaterenvironsci.com

Vibrational study of S(-) and R(+) forms of analgesic camphor combining DFT calculations with normal internal coordinates and SQMFF methodology

José Ruiz Hidalgo, Silvia Antonia Brandán*

Cátedra de Química General, Instituto de Química Inorgánica, Facultad de Bioquímica, Química y Farmacia, Universidad Nacional de Tucumán, Ayacucho 471, 4000, San Miguel de Tucumán, Tucumán, Argentina.

Received 13 July 2020,
Revised 27 Aug 2020,
Accepted 30 Aug 2020

Keywords
- ✓ *Camphor,*
- ✓ molecular structure,
- ✓ squamocin,
- ✓ DFT calculations,
- ✓ vibrational spectra.

Silvia Antonia Brandan :
brandansa@yahoo.com.ar

Abstract

B3LYP/6-311++G** calculations were performed to study structures and vibrational properties of *Cis* S(-) and R(+) forms of camphor. Comparisons between calculated geometrical parameters of both forms of Camphor in gas phase and aqueous solution show very good concordances with the experimental ones corresponding to (+)-3-bromocamphor. NBO calculations predict only $\Delta E_{\sigma\rightarrow\sigma^*}$, $\Delta E_{\sigma\rightarrow\pi^*}$ and $\Delta E_{n\rightarrow\sigma^*}$ interactions althougth the expected $\Delta E_{n\rightarrow\pi^*}$ transitions due to ketone groups C=O were no predicted. Gap and electrophilicity index (ω) values of both forms of camphor are close to the value observed in antiviral thymidine. Such observations could be explained by the proximities between the acceptor groups H bonds (C=O) and the CH_3 groups present in both camphor and thymidine species. Reasonable concordances were found among the predicted ^{1}H- and ^{13}C-NMR, UV-visible, ECD, IR and Raman spectra with the corresponding experimental ones. Complete vibrational assignments and scaled force constants for both forms camphor are reported for first time.

1. Introduction

In the present work, DFT calculations were performed to study structures and vibrational properties of two enantiomeric S(-) and R(+) forms of camphor because, so far, these properties are no reported. It cyclic monoterpene ketone is the main component of oil extracted from the wood of the camphor tree Cinnamomum Camphora (Linne) Nees et Ebermaier, family and is used in the medicinal chemistry due to its anti-inflammatory and analgesic properties among other multiple uses [1-33]. Camphor is known and investigated from long time and even today it is studied due to the side effects of its therapeutics uses and to its additional applications [26-33]. Moreover, studies related to the structural, electronic, topological and vibrational properties were no found in the literature and only studies on structure and electric dipole moment of camphor were determined by rotational spectroscopy [6] while camphor in CDCl3 was studied by VCD by Debie et al. [10]. Structurally, four enantiomers are expected for camphor due to its two chirals centers but only the cis forms are possible because the two trans forms are impossible from structural point of view [3]. Camphor is the generic name while its IUPAC name is

* Corresponding author. Tel.: +54-381-4247752; fax: +54-381-4248169;

E- mail: silvia.brandan@fbqf.unt.edu.ar (S.A. Brandán)

1,7,7-trimethylbicyclo[2.2.1]heptan-2-one. Both cis S(-) and R(+) structures of camphor showing the different positions of ketone group can be easily seen in Figure 1.

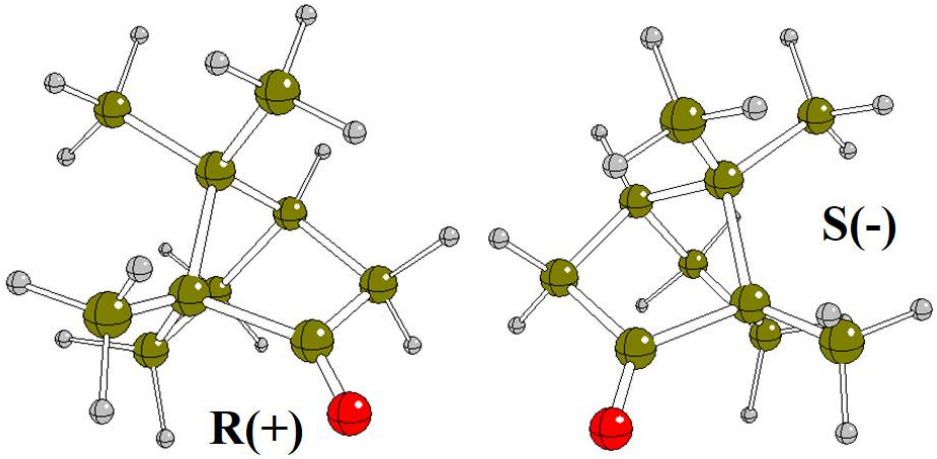

Figure 1: *Enantiomeric R(+) and S(-) structures of camphor.*

Taking into account the numerous studies reported on biological activities and few related with structural and vibrational studies, the aims of this work are:

(i) to perform the complete vibrational study of the two cis S(-) and R(+) forms of camphor combining the experimental available Attenuated Total Reflectance Infrared (ATR-IR) Spectrum and Raman spectra, the normal internal coordinates and DFT calculations with the SQMFF methodology and Molvib program [34-36],

(ii) (ii) to optimize the two enantiomers of camphor in gas phase and aqueous solution by using B3LYP/6-311++G** level of theory [37-41],

(iii) (iii) to compute the structural, electronic, topological and vibrational properties of both forms of camphor in the two media at the same level of theory, and finally,

(iv) (iii) to predict reactivities and behaviors of both cis S(-) and R(+) structures of camphor in the two media studied [42-45]. The reproducibility of theoretical optimized two cis S(-) and R(+) structures of camphor were verified comparing the predicted 1H- and 13C-NMR and UV-Vis spectra with the corresponding experimental ones available from the literature [3,4,46].

2. Material and Methods

The two *cis* S(-) and R(+) structures of camphor were modeled with the *GaussView* program [47] and, later, they were optimized in gas phase and aqueous solution by using the functional hybrid B3LYP/6-311++G** level of theory with the Revision A.02 of Gaussian 09 program [37,38,48]. Here, the integral equation formalism variant polarised continuum model (IEFPCM) method was used to optimize both forms in solution while with the universal solvation methods were predicted the solvation energies [39-41]. The properties in solution were studied with the self-consistent reaction field (SCRF) method and the volume variations that experiment both forms in aqueous solution were calculated with the Moldraw program [49]. The intra- molecular interactions were investigated by using the natural bond orbital (NBO) and atoms in molecules (AIM) 2000 programs [50-52] while the molecular electrostatic potentials were computed with the Merz-Kollman scheme [53]. The energy gap values for both forms were calculated with the frontier orbitals and, then, with these values were also calculated the chemical potential (μ), electronegativity (χ), global hardness (η), global softness (S), global electrophilicity index (ω) and global nucleophilicity index (E) descriptors [42-45]. Time-dependent DFT calculations (TD-

DFT) together with the GIAO method were employed to predict the ultraviolet-Visible and ^{1}H and ^{13}C NMR spectra in aqueous solution at the same level of theory [54]. Here, the scaled mechanical force field (SQMFF) procedure with the Molvib program were used to perform the complete vibrational assignments of those two forms of camphor. In the determination of force fields in both media, the normal internal coordinates and transferable scaling factors were employed considering potential energy distribution (PED) contributions ≥ 10 % [35]. Finally, known equations were used to transform the Raman spectra from activities to intensities [55,56].

3. Results and Discussion

3.1. Optimizations and properties in both media

Figure 2 shows the optimized structures of both S(-) and R(+) forms of camphor together with the atoms labelling. In both structures of camphor the C3 and C4 atoms are chirals centers but only the *cis* conformations S(-) and R(+) can exist with the cyclohexane ring (C8-C3-C5-C6-C4-C7) in boat form because the gem-dimethyl bridge formed by the C3-C2-C4 atoms should necessarily be *cis*. Hence, in **Figure 3** it is possible to see that the fundamental skeleton of camphor is bicyclic with a six membered carbon-ring and two five members' rings together with the involved atoms.

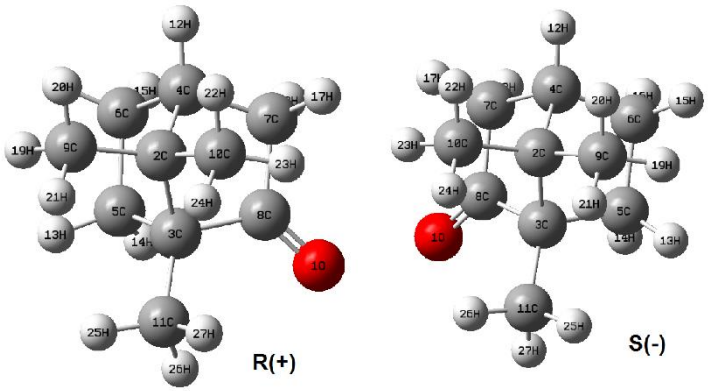

Figure 2. Optimized structures of both S(-) and R(+) forms of camphor with the atoms labelling.

The definitions of three rings are presented in **Figure 3** where R1 is the ring of five members observed in green colour (C2-C4-C7-C8-C3), R2 is the other five members ring formed by the C2-C4-C6-C5-C3 atoms and R3 is the cyclohexane ring in boat form observed in yellow colour in Fig. 4. The atoms in R3 are: C8-C3-C5-C6-C4-C7.

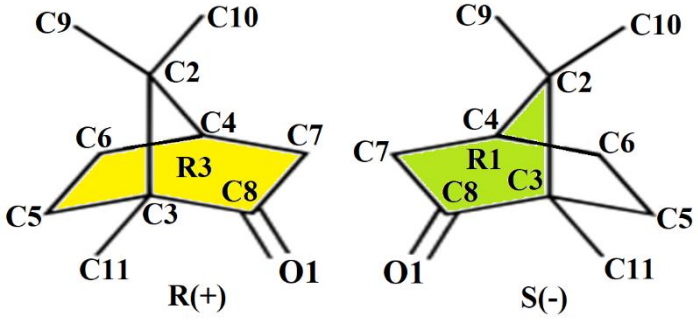

Figure 3. Definitions of three rings in both S(-) and R(+) forms of camphor with the involved atoms.

Calculated geometrical parameters of both S(-) and R(+) forms of Camphor in gas phase and aqueous solution by using hybrid B3LYP/6-311++G** method are presented in **Table 1** compared with the experimental values corresponding to crystal structure of (+)-3-bromocamphor determined by Allen and Rogers [2].

Table 1. Comparison of calculated geometrical parameters of S(-) and R(+) forms of Camphor in gas phase and aqueous solution by using the B3LYP/6-311++G** method with the corresponding experimental ones taken from Ref [2]. Very

Parameters	B3LYP/6-31G* Method				Experimental[b]
	R(+)		S(-)		
	Gas	Water	Gas	Water	
	Bond lengths (Å)				
O1-C8	1.207	1.222	1.207	1.222	1.20
C8-C3	1.534	1.520	1.534	1.520	1.54
C3-C11	1.516	1.515	1.516	1.515	1.52
C3-C5	1.566	1.571	1.566	1.571	1.49
C5-C6	1.558	1.556	1.558	1.556	1.56
C6-C4	1.546	1.545	1.546	1.545	1.57
C4-C7	1.541	1.542	1.541	1.542	1.46
C7-C8	1.535	1.522	1.535	1.522	1.54
C3-C2	1.573	1.575	1.573	1.575	1.53
C2-C4	1.565	1.564	1.565	1.564	1.54
C2-C9	1.536	1.534	1.536	1.534	1.55
C2-C10	1.539	1.538	1.539	1.538	1.54
RMSD[b]	**0.036**	**0.039**	**0.036**	**0.039**	
O1-C8-C3	126.99	126.70	126.99	126.71	127.7
O1-C8-C7	126.48	126.05	126.48	126.05	126.6
C8-C3-C11	114.54	115.44	114.54	115.43	112.3
C8-C3-C5	102.92	102.49	102.92	102.47	102.8
C8-C3-C2	100.47	100.38	100.47	100.38	100.8
C8-C7-C4	101.96	101.90	101.96	101.91	102.0
C3-C5-C6	104.44	104.54	104.44	104.54	104.1
C3-C2-C4	93.81	93.78	93.81	93.78	94.9
C5-C6-C4	102.73	102.66	102.73	102.67	104.1
C6-C4-C7	106.57	106.45	106.57	106.47	111.4
C7-C8-C3	106.53	107.23	106.53	107.22	105.6
C6-C4-C2	102.74	102.81	102.74	102.80	98.3
C7-C4-C2	102.66	102.46	102.66	102.46	103.2
C4-C2-C9	113.65	113.85	113.65	113.84	113.8
C4-C2-C10	114.11	114.31	114.11	114.30	112.6
C3-C2-C9	114.27	113.93	114.27	113.95	112.2
C3-C2-C10	113.36	113.26	113.36	113.27	112.3
C9-C2-C10	107.41	107.47	107.41	107.47	110.3
C5-C3-C2	101.92	101.78	101.92	101.79	102.6
C5-C3-C11	114.99	114.91	114.99	114.90	115.7
C2-C3-C11	119.56	119.30	119.56	119.30	120.5
RMSD[b]	**1.820**	**1.934**	**1.820**	**1.929**	
O1- C8-C3-C11	16.99	17.06	-17.01	-17.06	
O1- C8-C7-C4	178.86	178.79	-178.85	-178.78	
C11-C3-C2-C10	61.01	61.47	62.53	61.79	
C11-C3-C5-C6	162.96	162.05	-162.98	-162.06	
C11-C3-C2-C4	179.36	-179.99	-179.35	179.99	

[a]This work, [b]Ref [2]

These comparisons are presented in the same table in terms of root-mean-square deviation (RMSD) values. Very good correlations are observed in the bond lengths and angles of both enantiomers showing

the same RMSD values in both media (0.036 Å and 1.820º in gas phase and 0.039 Å and 1.929º in aqueous solution). However, the only differences expected between both forms are in the dihedral angles because the O1-C8-C3-C11, O1-C8-C7-C4 and C11-C3-C5-C6 angles present positive signs in R(+) while negative signs in S(-). Moreover, the dihedral C11-C3-C2-C4 angles in both forms have different signs in the two media; hence, in gas phase that angle has positive sign in R(+) while in solution negative. A contrary resulted it is observed for the S(-) form, as can be seen in Table 1. Evidently, the presence of CH_3 groups closer the C8=O1 bonds could have some influence in the hydration of the two forms in aqueous solution because the C=O group is acceptor of H bonds. For these reasons, the studies for both forms in solution are necessaries in order to understand why those dihedral angles in the R(+) and S(-) forms change of signs in this medium. In **Table 2** are presented the C11⋯O1 and O1⋯H distances between the H26 and H27 atoms of CH_3 groups (C11) more closer to O1 atoms in both forms and in the two media by using the hybrid B3LYP/6-311++G** method. Analyzing the results we can see clear differences in the O1⋯H26 and O1⋯H27 distances of both forms in the two media between the H26 and H27 atoms of CH_3 groups (C11) more closer to O1 atoms by using the hybrid B3LYP/6-311++G** method. The positions of H26 and H27 atoms in the R(+) form is different from the S(-) one and, hence, the change of signs observed in both media.

Table 2. Distances between the H26 and H27 atoms of CH_3 groups (C11) more near to O1 atoms in both S(-) and R(+) forms by using the the hybrid B3LYP/6-311++G** method.

B3LYP/6-311++G** method[a]				
Distances	R(+)		S(-)	
	Gas	PCM	Gas	PCM
C11⋯O1	2.940	2.948	2.940	2.948
O1⋯H26	3.047	3.026	2.807	2.867
O1⋯H27	2.807	2.869	3.047	3.028

[a]This work

Calculated total uncorrected and corrected by zero point vibrational energy (ZPVE) energies, dipole moments and volumes of S(-) and R(+) forms of camphor in gas phase and aqueous solution by using the B3LYP/6-311++G** method are observed in **Table 3** while the solvation energies for both forms in aqueous solution can be seen in **Table 4**.

Table 3. Calculated total uncorrected and corrected by ZPVE energies (*E*), dipole moments (μ) and volumes (V) of S(-) and R(+) forms of Camphor in gas phase and aqueous solution by using the B3LYP/6-311++G** method.

B3LYP/6-311++G** Method					
Medium	E (Hartrees)	E_{ZPVE} (Hartrees)	μ (D)	V (Å^3)	ΔV
Conformacion R(+)					
GAS	-466.0523	-465.8124	3.29	181.5	0.3
PCM/Water	-466.0594	-465.8202	5.10	181.8	
Conformacion S(-)					
GAS	-466.0523	-465.8124	3.29	182.5	-0.5
PCM/Water	-466.0594	-465.8202	5.10	182.0	

The results from **Table 3** show the same energy values for both forms in the two media, an unexpected result considering that both conformations are enantiomers and the images are not superimposable. Only differences in the dipole moment values for the two forms in solution and a slight variation in the volumes in this medium are observed. Note that the dipole moment values calculated in gas phase for both forms are in agreement with that determined for camphor from Stark effect measurements $\mu_{tot} = 3.0821(22)$ D by Kisiel et al. [6]. Here, the S(-) form shows expansion of volume in solution while

the R(+) one evidence a slight contraction in the volume. Hence, differences between both forms can be observed in solution in the solvation energy values shown in **Table 4** where the R(+) form (-39.65 kJ/mol) presents a higher value than the other one (-37.56 kJ/mol). The changes of signs predicted in the dihedral C11-C3-C2-C4 angles of both forms in the two media could explain the different solvation energy values and the different positions of H atoms of CH_3 groups in relation to O1 atoms of C8=O1 bonds.

Table 4. Corrected and uncorrected solvation energies by the total non-electrostatic terms and by zero point vibrational energy (ZPVE) of S(-) and R(+) forms of Camphor in gas phase and aqueous solution by using the B3LYP/6-311++G** method.

B3LYP/6-311++G** method[a]			
Solvation energy (kJ/mol)			
Medium	$\Delta G_{un}^{\#}$	ΔG_{ne}	ΔG_c
Conformacion R(+)			
PCM/Water	-20.46	19.19	-39.65
Conformacion S(-)			
PCM/Water	-18.62	18.94	-37.56

$\Delta G_{un}^{\#}$= uncorrected solvation energy, ΔG_{ne}= total non electrostatic terms, ΔG_c= corrected solvation energies.

The $\Delta G_{un}^{\#}$ uncorrected solvation energy value is defined as the difference between the total energies in aqueous solutions and the values in gas phase, the ΔG_{ne} values correspond to total energy non electrostatic terms due to the cavitation, dispersion and repulsion energies while the corrected ΔG_c values solvation energies are those calculated as the difference between the uncorrected and non-electrostatic solvation energies. When the dipole moments vectors of both forms in gas phase are graphed in **Figure 4** we observed practically the same magnitudes, orientations and directions of both vectors. Hence, probably the differences in the volumes in addition to different dihedral C11-C3-C2-C4 angles in both forms could justify the different ΔG_c values observed in both enantiomers.

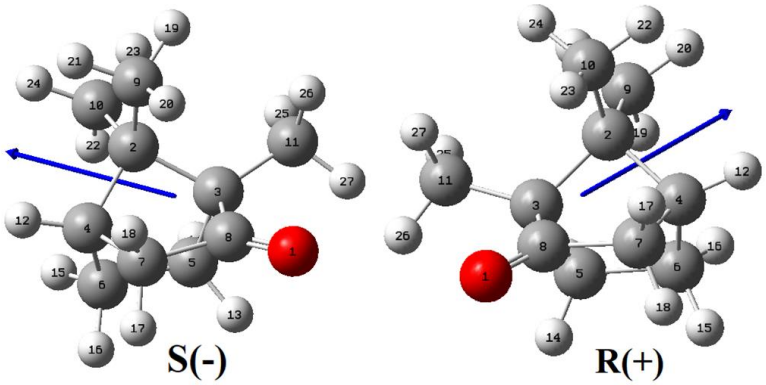

Figure 4. Magnitudes and positions of dipole moments vectors of the two enantiomeric S(-) and R(+) forms of Camphor in gas phase by using hybrid B3LYP/6-311++G** method.

3.2. Atomic charges, molecular electrostatic potentials (MEP) and bond orders (BO) studies

Atomic Merz-Kollman (MK), Mulliken and natural population atomic (NPA) charges were studied in both R(+) and S(-) forms of camphor in gas phase and aqueous solution by using the B3LYP/6-311++G** method because the dihedral angles and the solvation energies have evidenced different behaviours between both enantiomers in solution. Besides, it is very important to undestand the conexion existent between the only acceptor H bonds group (O) in both R(+) and S(-) forms and the different properties attributed from long time to camphor [3,7,8,11-15,17-21,23-29]. Hence, atomic Merz-Kollman (MK), Mulliken and natural population atomic (NPA) charges were studied together with the

molecular electrostatic potentials (MEP) and bond orders (BO) for both forms of camphor in both media by using the the B3LYP/6-311++G** method. These properties are presented in **Tables S1** and **S2** of supporting material. In the analyses of these properties only the O1, C11, H25, H26 and H27 atoms were considered because the above studies have suggested that the proximities between the CH_3 and C8=O1 groups justify the variations observed in the solvation energies and dihedral C11-C3-C2-C4 angles of two R(+) and S(-) forms. **Figure 5** shows the behaviours of three charges on those five atoms of two enantiomeric R(+) and S(-) forms of camphor in aqueous solution by using hybrid B3LYP/6-311++G** method. Regarding Fig. 5 it is observed similar behaviours on five atoms of both forms in solution although the three types of charges for a same atom evidence different values.

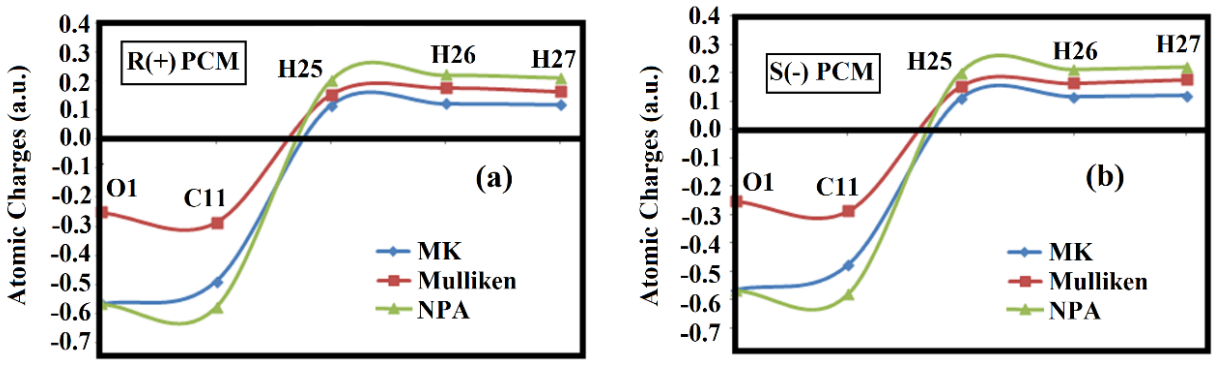

Figure 5. Variations in the atomic Merz-Kollman (MK), Mulliken and natural population atomic (NPA) charges of the two enantiomeric: (a) R(+) and (b) S(-) forms of Camphor in aqueous solution by using hybrid B3LYP/6-311++G** method.

Hence, the MK, Mulliken and NPA charges on the H atoms present the higher positive values while the higher negative values are evidenced in the MK charges on O1 atoms of both forms (blue lines). On the contrary, the Mulliken and NPA charges show higher negative values on C11 atoms (red and green lines, respectively), as compared with the observed on O1 atoms. The MK charges on the three H atoms present the lower values in relation to the other ones while the higher values are observed in the NPA charges on those three H25, H26 and H27 atoms.

Molecular electrostatic potentials (MEP) values calculated from MK charges for both R(+) and S(-) forms of camphor in the two media by using hybrid B3LYP/6-311++G** method are observed in Tables S1 and S2 [53]. Analyzing particularly these MEP surfaces only on the five O1, C11, H25, H26 and H27 atoms we observed the same values on the O1, C11 and H25 atoms of both forms in the two media but, the MEPs values on the H26 and H27 atoms show different values in both forms and in the two studied media. Hence, these results are in agreement with the differences observed in both forms in the values of solvations energies and in the dihedral C11-C3-C2-C4 angles. These mapped MEP surfaces of R(+) and S(-) forms are also interesting to see the nucleophilic and electrophilic sites where the reaction with electrophils and nucleophils potential biological reactive take place. The mapped MEP surfaces of R(+) and S(-) forms in gas phase are presented in **Figure S1**. As expected, due to only acceptor H bonds (O1 atoms) in both forms strong red colours are observed on the C8=O1 bonds in both forms while on the H atoms of CH_3 groups slight light blue colours are observed. Evidently, the strong red colours are nucleophilic sites, the soft blue colours electrophilic places while the green colours are inert regions.

Other interesting property studied in both R(+) and S(-) forms of camphor in gas phase and aqueous solution by using the B3LYP/6-311++G** method are the bond orders, expressed as Wiberg indexes. In Tables S1 and S2 are presented these results for all atoms of two species of camphor. When the BOs

values are analyzed only for the O1, C11, H25, H26 and H27 atoms it is observed that the O1, C11 and H25 atoms of both forms in the two media present the same values but, the BOs values on the H26 and H27 atoms show different values in both R(+) and S(-) forms and in the two studied media, as as previously observed in studies of atomic charges and electrostatic potentials. Hence, the three properties studied in this section justify the differences observed between both forms in the values of solvations energies and in the dihedral C11-C3-C2-C4 angles.

3.3. NBO and AIM studies

Calculations of Second Order Perturbation Theory Analysis of Fock Matrix in NBO Basis by using the NBO programa are of great interest to investigate donor-acceptor energy interactions while the topological properties calculated from the Bader'theory of atoms in molecules (AIM) allows to predict intra-molecular or H bonds interactions [50-52]. These two type of calculations were performed for both R(+) and S(-) forms of camphor in gas phase and aqueous solution by using the B3LYP/6-311++G** method. Hence, in **Table S3** are summarized the main delocalization energies (in kJ/mol) of R(+) and S(-) forms of camphor in gas phase and aqueous solution by using B3LYP/6-311++G** calculations. The analyses of results show the same three interactions in both forms which are the $\Delta E_{\sigma\rightarrow\sigma^*}$, $\Delta E_{\sigma\rightarrow\pi^*}$ and $\Delta E_{n\rightarrow\sigma^*}$ interactions where the former interactions are performed from bonding σ C-C and C-H orbitals to antibonding σ C=O, C-C and C-H orbitals, the second ones from bonding σC-C and C-H orbitals to antibonding πC=O orbitals and, the latter interactions are performed from lone pairs of O1 atoms to antibonding σC-C orbitals. Note that the interactions of higher energies in both forms are the $\Delta E_{\sigma\rightarrow\sigma^*}$ interactions. The higher values observed in total energies of both forms evidence higher stabilites of two forms of camphor in gas phase (542.49 kJ/mol), as compared with the values obtained in aqueous solution (536.94 kJ/mol).

Other studied properties in this section to investigate different intra-molecular or H bonds interactions in the two forms of camphor are the topological properties according to the Bader's theory of atoms in molecules (AIM) with the AIM 2000 program [51,52]. Hence, the electron density distribution, $\rho(r)$, the Laplacian values, $\nabla^2\rho(r)$, the eigenvalues $(\lambda1, \lambda2, \lambda3)$ of the Hessian matrix and the $\lambda1/\lambda3$ ratio were computed for both R(+) and S(-) forms of camphor in gas phase and aqueous solution by using the B3LYP/6-311++G** method. These properties should be calculated in the bond critical points (BCPs) and in the ring critical points (RCPs) and are presented for both R(+) and S(-) forms of camphor in the two media in **Table S4**. Here, the results for both forms have not evidenced new BCPs with values of $\lambda1/\lambda3 < 1$ and $\nabla^2\rho(r) > 0$ and, for these reasons, only the RCPs are presented in Table S4. These RCPs are observed only in the two five members rings, where RCP1 correspond to R1 ring and RCP2 correspond to R2 ring. In **Figure S2** can be observed the molecular graphics of R(+) and S(-) forms of camphor in gas phase showing only those two ring critical points (RCPs). The properties presented in Table S4 show the same values for the R(+) and S(-) forms in both media but slightly different in solution, as was also observed in the above studies. RCP1 and RCP2 present different topological properties in R(+) and S(-) forms in the two media but the same values in gas phase and in aqueous solution.

3.4. Frontier orbitals and global descriptors

The knowledge of the energies gap and of some typical descriptors in the two R(+) and S(-) forms of camphor are essential to predict their reactivities and behaviours in different media taking into account the diverse medicinal and biological properties attributed to camphor [3,7,8,11-15,17-21,23-29]. Hence, the frontier orbitals and the chemical potential (μ), electronegativity (χ), global hardness (η), global

softness (*S*), global electrophilicity index (ω) and nucleophilicity indexes (*E*) descriptors were calculated for the two R(+) and S(-) forms of camphor in gas phase and aqueous solution by using the hybrid B3LYP/6-311++G** method [42-45]. Therefore, the calculated HOMO and LUMO, energy band gaps and those mentioned descriptors are presented for both forms of camphor in gas phase and aqueous solution in **Table S5** together with the equations used to compute the descriptors. Analyses of gap values show that both forms are less reactive in gas phase because they have high energy values, however, the energy gaps slightly decrease in both forms in solution increasing their reactivities from 5.9006 eV gas phase to 5.8535 eV in solution. The same energy gap values observed for both forms in the two studied media show that there are no differences in the reactivities between both enantiomers and that the two can exist in both media. These gap values for both forms of camphor in solution are compared with those reported for antiviral isothiazol, thymidine and chloroquine and anti-histaminic promethazine agent [44,45,57,58] in **Table S6** while in **Figure S3** can be observed the molecular structures of all compared compounds. Comparing the gap values, we observed that the two forms of camphor are less reactive than the other ones while the most reactive species with low gap value is the S(-) form of chloroquine (4.2994 eV). Note that the gap values for both forms of camphor are close to the value observed in thymidine (5.4748 eV). If now the the electrophilicity index (ω) are compared among all species it is observed that the values of two forms of camphor (2.3229 eV) are close to that observed for thymidine (2.0728 eV). The proximity between the acceptor groups H bonds (C=O) and the CH_3 groups in both camphor and thymidine species (see Fig. S3) probably justifies the close gap and ω values. Whereas if the the nucleophilicity indexes (*E*) of all species are compared the values for camphor (-10.7920 eV) are close to value of isothiazol (-10.0022 eV). This observation could possibly be justified by the absence of donors H bonds in camphor and isothiazol (S-H is very weak) or maybe by the fused six and five members rings.

3.5. NMR studies

To perform the vibrational study it is necessary to known the reproducibility of both structures and, for these reasons, the theoretical ^{1}H and ^{13}C NMR spectra were predicted for the two R(+) and S(-) forms of camphor and compared with the experimental available from the literature by using the root-mean-square deviation (RMSD) values. The predicted ^{1}H and ^{13}C NMR spectra of both R(+) and S(-) forms of camphor were obtained by using by using the B3LYP/6-311++G** and GIAO methods [54] and they are compared with the corresponding experimental ones available from Refs [3,4] in $CDCl_3$ solution. Comparisons of chemical shifts for both forms can be seen in **Tables S7** and **S8** by using RMSD values. Low RMSD values and very good correlations for both forms in gas phase and aqueous solution are observed in the chemical shifts of H atoms with similar values (0.25-0.24 ppm). However, when the chemical shifts of C atoms are compared reasonable correlations are obtained (10.59-10.29 ppm). These differences can be attributed to the calculations because the B3LYP/6-311++G** method perform better calculations for the H nuclei than the C ones, as observed in other species [59-61]. The similar values observed in the chemical shifts of H and C atoms of both forms of camphor in solution probably suggest the presence of both enantiomers in solution and, hence, both forms could be present as a racemic structure in the solid phase. Hence, the vibrational studies should be performed for the two R(+) and S(-) forms of camphor.

3.6. Vibrational study

Both structures R(+) and S(-) forms of camphor were optimized by using B3LYP/6-311++G** calculations with C_1 symmetries and due to the presence of 27 atoms the number of expected vibration

modes are 75. All these modes present activity in both infrared and Raman spectra. The normal internal coordinates of three rings, two of them are five members rings (R1 and R2) and the other one of six members (R3) were built according to the definitions presented in **Figure 3.** Experimental available infrared in transmittance mode, attenuated total reflectance (ATR) and Raman spectra of camphor in the solid phase were taken from the literature [46] and they are compared in **Figures 6** and **7** with the corresponding predicted for the R(+) and S(-) forms of camphor in gas phase.

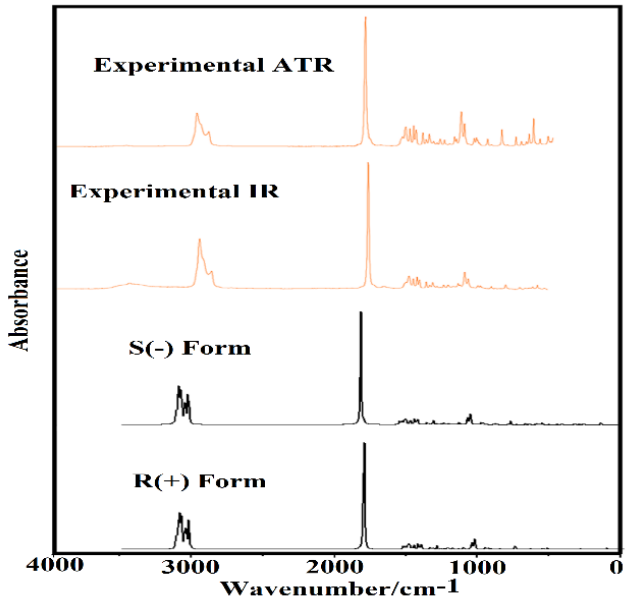

Figure 6. Experimental available Infrared spectra of camphor in solid phase [46] compared with the predicted for the S(-) and R(+) forms in gas phase by using the hybrid B3LYP/6-311++G** method.

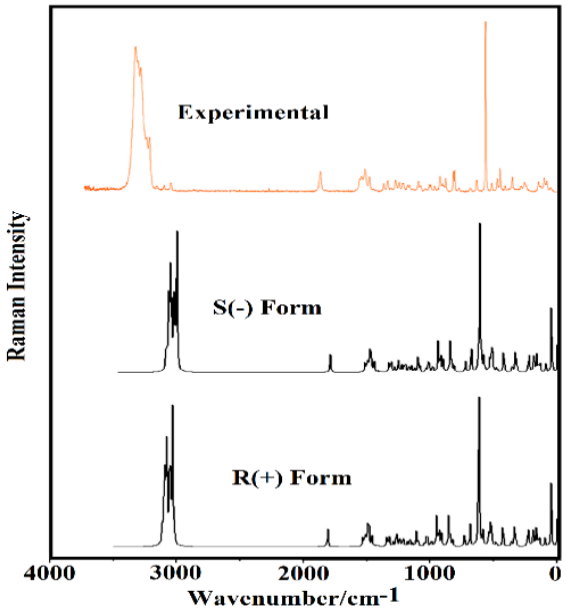

Figure 7. Experimental available Raman spectra [46] compared with the predicted for the S(-) and R(+) forms in gas phase by using the hybrid B3LYP/6-311++G** method.

Very good correlations were found in the positions and intensities of observed bands between experimental and theoretical ones, as can be seen in those two figures. The predicted Raman spectra of both froms were corrected to intensities for a better correlation [55,56]. The harmonic force fields for both species of camphor were calculated by using the scaled quantum mechanical force field (SQMFF) methodology, normal internla coodinates, scaling factors and the Molvib program [34-36]. Potential energy distribution (PED) contributions ≥ 10% were considered in the assignments of bands observed to the normal vibration modes. In **Table 5** are presented observed and calculated wavenumbers for the R(+) and S(-) forms of camphor in gas phase by using B3LYP/6-311++G** calculations together with their corresponding assignments. Discussions on some important assignments are presented below.

3.6.1. Band Assignments

3.6.1.1. 4000-2000 cm^{-1} region. Both R(+) and S(-) forms of camphor have three CH_3 (C9, C10 and C11) and three CH_2 (C5, C6 and C7) groups and, for these reasons, the antisymmetric and symmetric stretching modes corresponding to these groups, in addition to aliphatic C4-H12 groups, are expected in this region. In compounds containing these groups, the stretching modes of CH_3 and CH_2 groups are assigned between 3090/2914 and 2970/2842 cm^{-1}, respectively [43-45,57-61]. Hence, the antisymmetric and symmetric stretching modes of CH_3 and CH_2 are assigned as predicted by SQM calculations between 2988/2899 and 2969/2921 cm^{-1}, respectively. Note that the complete vibrational assignments are practically the same for both forms while the only differences predicted by SQM calculations correspond

to the antisymmetric and symmetric stretching modes of gem-dimethyl bridge (C9 and C10 atoms) in both R(+) and S(-) forms which are predicted exchanged, as can be seen in **Table 5.** The aliphatic C4-H12 groups of both forms is assigned as predicted by calculations to the intense IR band at 2948 cm^{-1}.

Table 5. Observed and calculated wavenumbers (cm^{-1}) and assignments for R(+) and S(-) forms of Camphor in gas phase by using the B3LYP/6-311++G** method.

Exp[b]		B3LYP/6-311++G** method[a]			
		R(+)		S(-)	
IR	Raman	SQM[c]	Assignments[a]	SQM[c]	Assignments[a]
2961s	2988vs	2988	ν_aCH_3(C10)	2988	ν_aCH_3(C9)
2941sh		2976	ν_aCH_3(C9)	2976	ν_aCH_3(C10)
	2972sh	2969	ν_aCH_2(C6)	2969	ν_aCH_2(C6)
		2968	ν_aCH_3(C11)	2968	ν_aCH_3(C11)
		2964	ν_aCH_3(C11)	2964	ν_aCH_3(C11)
		2961	ν_aCH_2(C7)	2961	ν_aCH_2(C7)
	2953s	2955	ν_aCH_3(C9)	2955	ν_aCH_3(C10)
		2951	ν_aCH_2(C5)	2951	ν_aCH_2(C5)
2948s		2948	νC4-H12	2948	νC4-H12
		2948	ν_aCH_3(C10)	2948	ν_aCH_3(C9)
	2929sh	2930	ν_sCH_2(C6)	2930	ν_sCH_2(C6)
		2927	ν_sCH_2(C7)	2927	ν_sCH_2(C7)
2917sh		2921	ν_sCH_2(C5)	2921	ν_sCH_2(C5)
		2906	ν_sCH_3(C10)	2906	ν_sCH_3(C9)
		2903	ν_sCH_3(C11)	2903	ν_sCH_3(C11)
2877w	2889s	2899	ν_sCH_3(C9)	2899	ν_sCH_3(C10)
1743vs	1751m	1737	νC8=O1	1737	νC8=O1
1471w	1476m	1464	δCH_2(C6)	1464	δCH_2(C6)
1453sh	1452m	1453	δCH_2(C5), δ_aCH_3(C9)	1453	δCH_2(C5), δ_aCH_3(C9)
1445m	1444sh	1449	δ_aCH_3(C9)	1449	δ_aCH_3(C10)
1439sh		1438	δCH_2(C5) δ_aCH_3(C9)	1438	δ_aCH_3(C10)
		1434	δ_aCH_3(C11)	1434	δ_aCH_3(C11)
1422sh		1428	δ_aCH_3(C10)	1428	δ_aCH_3(C11)
		1423	δ_aCH_3(C11)	1423	δ_aCH_3(C11), δ_aCH_3(C11)
1418m	1420m	1420	δ_aCH_3(C10)	1420	δ_aCH_3(C9)
1390m	1392vw	1395	δCH_2(C7)	1395	δCH_2(C7)
1372m	1378vw	1364	δ_sCH_3(C9)	1364	δ_sCH_3(C10)
		1349	δ_sCH_3(C11)	1349	δ_sCH_3(C11)
1332sh	1326w	1343	δ_sCH_3(C10)	1343	δ_sCH_3(C9)
1324m		1313	wagCH_2(C5)	1313	wagCH_2(C5)
1318sh	1204sh	1305	wagCH_2(C6)	1305	wagCH_2(C6)
1280w	1298w	1289	ρ'C4-H12	1289	ρ'C4-H12
1247w	1276vw	1258	ρC4-H12	1258	ρC4-H12
1240sh	1248w	1240	wagCH_2(C7), νC4-C7 ρCH_2(C5)	1240	wagCH_2(C7),νC4-C7 ρCH_2(C5)
1222w	1221w	1233	τR_1(A1)	1233	τR_1(A1)
1197w	1199w	1209	ρCH_2(C6)	1209	ρCH_2(C6)
	1193w	1188	τR_2(A1)	1188	τR_2(A1)
1169w	1169w	1174	τR_3(A3),τR_2(A1)	1174	τR_3(A3),τR_2(A1)
1163sh	1152w	1153	ρCH_2(C7),ρC4-H12 ρCH_3(C11)	1153	τR_2(A3) νC3-C11
1127w	1131vw	1120	τR_2(A1), τR_1(A2)	1120	τR_2(A1), τR_1(A2) ρ'CH_3(C11)
1095w	1093w	1109	τR_3(A3), τR_1(A2)	1109	τR_3(A3), τR_1(A2)
1075w	1079w	1087	ρ'CH_3(C11)	1087	ρCH_3(C11)
1047s	1047vw	1066	τR_1(A2)	1066	τR_1(A2)

1022m	1022w	1014	τR$_1$(A2),τR$_2$(A1)	1014	τR$_1$(A2), τR$_2$(A2)
990vw	1011w	997	ρCH$_3$(C10)	997	ρ'CH$_3$(C9),ρ'CH$_3$(C10)
960sh	986w	982	τR$_1$(A2),τR$_2$(A1)	982	τR$_1$(A2), τR$_2$(A2)
952w	950m	963	τR$_3$(A3), τR$_1$(A2)	963	τR$_3$(A3), τR$_1$(A2)
934w	934w	929	ρ'CH$_3$(C9), νC2-C10 ρ'CH$_3$(C10) ρCH$_3$(C9)	930	ρCH$_3$(C10), νC2-C9 ρCH$_3$(C9)
926w	926sh	924	νC2-C9	924	νC2-C10
915w	914w	907	νC5-C6	907	νC5-C6
858sh	862s	888	τR$_3$(A3), τR$_1$(A2)	888	τR$_3$(A3), τR$_1$(A2)
855w	850s	874	τR$_3$(A3),τR$_2$(A1)	874	τR$_3$(A3), τR$_2$(A1)
848sh	846sh	831	νC4-C6	831	νC4-C6
829w	822w	822	νC3-C5	822	νC3-C5
751m	772vw	776	τR$_2$(A3),τwCH$_2$(C6)	776	τR$_2$(A3), τwCH$_2$(C6)
709vw	747w 706w	703	τwCH$_2$(C5), νC2-C3 νC3-C8	703	τwCH$_2$(C5), νC2-C3 νC3-C8,τwCH$_2$(C7)
647w	648vs	678	νC2-C4	678	νC2-C4
610w	604w	622	νC3-C11,νC7-C8 βC8=O1	622	νC3-C11,νC7-C8 βC8=O1
574w	568w	588	τR$_2$(A1), γC8=O1	588	τR$_2$(A1), γC8=O1
552w	549s	553	τR$_3$(A3),τR$_2$(A1)	553	τR$_3$(A3),τR$_2$(A1)
521s	530vw	538	τR$_1$(A2), τR$_1$(A1)	538	τR$_1$(A2), τR$_1$(A1)
514sh	515w	511	τR$_1$(A2)	511	τR$_1$(A2)
472w	468m	464	τR$_2$(A2)	464	τR$_2$(A2)
415w	410w	402	τR$_1$(A3)	402	τR$_1$(A2),τR$_2$(A1)
	386w	389	δC10C2C9,δC9C2C3 δC10C2C4 δC9C2C4	389	δC9C2C3,δC10C2C9 δC9C2C4 δC10C2C4
	375sh	373	τR$_1$(A2)τR$_2$(A1) δC11C3C5	373	τR$_1$(A2)τR$_2$(A1) δC11C3C5
	292w	292	τR$_1$(A2),τR$_3$(A3)	292	τR$_1$(A2),τR$_3$(A3)
	281w	284	τR$_1$(A2)	284	τR$_3$(A3), τR$_1$(A2)
	254m	256	τR$_3$(A3)	256	τR$_3$(A3), τR$_1$(A2)
	237w	236	τR$_1$(A2),τR$_3$(A3) δC11C3C2	236	τR$_1$(A2),τR$_3$(A3) δC11C3C2
	210w	209	τR$_3$(A3), τR$_1$(A2)	209	τR$_3$(A3)
	197sh	200	τwCH$_3$(C9),τwCH$_3$(C10) τwCH$_3$(C11)	200	τwCH$_3$(C10), τwCH$_3$(C9)
		156	τR$_3$(A3), τR$_1$(A2)	156	τR$_3$(A3), τR$_1$(A2) τwCH$_3$(C11)
		150	τR$_1$(A2),τR$_3$(A3)	150	τR$_1$(A2),τR$_3$(A3)
		106	τR$_3$(A3),τR$_2$(A1)	106	τR$_3$(A3)

Abbreviations: ν, stretching; β, deformation in the plane; γ, deformation out of plane; wag, wagging; τ , torsion; β$_R$, deformation ring τ$_R$, torsion ring; ρ, rocking; τw, twisting; δ, deformation; a, antisymmetric; s, symmetric; (A$_1$), Ring 1; (A$_2$), Ring 2; (A$_3$), Ring 3; [a]This work, [b]From Ref [46], [c]From scaled quantum mechanics force field.

3.6.1.2. 2000-1000 cm^{-1} region. Both forms of camphor predict a very intense band typical of C8=O1 stretching modes and, for these reasons, the very strong IR band at 1743 is clearly assigned to those vibration modes of R(+) and S(-) forms. Then, the deformation, wagging and rocking modes of CH_3 and CH_2 groups are also predicted in this region. Hence, the groups of IR and Raman bands between 1476 and 1075 cm^{-1} are assigned to antisymmetric and symmetric deformation and rocking modes of CH_3 and to deformation, wagging and rocking modes of CH_2 groups, as predicted by calculations and, as detailed in Table 5. The two rocking modes of aliphatic C4-H12 groups are predicted in the same regions for both forms of camphor and, hence, they are assigned to the weak IR bands at 1280 and 1247 cm^{-1}. Note that some vibrations corresponding to torsions of three rings are also predicted in this region. Other

important observation is that the C4-C7 stretching modes are the only C-C stretching predicted in this region which is assigned to the weak Raman band at 1248 cm^{-1}.

3.6.1.3. 1000-20 cm^{-1} region. In this region, the very strong Raman band at 648 cm^{-1} is assigned to the C2-C4 stretching modes, as predicted the SQM calculations for the R(+) and S(-) forms of camphor. On the other hand, some CH_3 rocking and twisting modes are predicted in this region together with the other C-C stretching modes, deformations and torsions modes of three rings and skeletal modes corresponding to C8=O1 groups. All these vibration mode are assigned according the SQM calculations performed here and, taking into account assignments of compounds with similar groups [43-45,57-61].

4. Force fields

The SQMFF methodology and the Molvib program have allowed the determination of harmonic force fields for both R(+) and S(-) forms of camphor and, also, of the corresponding scaled force constants [34-36]. These parameters are necessary to predict the force of bonds and, for these reasons, they were calculated for both forms of camphor in gas phase and aqueous solution by using the B3LYP/6-311++G** method. The results for both forms in the two studied media are presented in **Table 6**. We can see that the scaled force constants values are the same for both forms and in the two media and, only a slight difference in the *f(νC-C)* force constants are observed in solution between the R(+) and S(-) forms. Besides, in solution the C8=O1 bonds in both forms are hydrated because the corresponding force constants values present a diminishing in solution, as expected because these groups are acceptors H bonds. These studies show clearly that both forms can exist in solution, as also suggest the above studies performed in this work. Comparisons between the *f(νCH₃)* and *f(νCH₂)* force constants of both forms of camphor with those calculated for promethazine (4.90/4.82 and 4.85/4.74 mdyn $Å^{-1}$) and chloroquine (4.78 and 4.63/4.57 mdyn $Å^{-1}$) show good concordances [44,58].

Table 6. Scaled internal force constants for both R(+) and S(-) forms of Camphor in gas phase and aqueous solution by using the B3LYP/6-311++G** method.

Force constant	B3LYP/6-311++G** method[a]			
	Camphor			
	Gas Phase		Aqueous Solution	
	R(+)	S(-)	R(+)	S(-)
f(νC-H)	4.80	4.80	4.80	4.80
f(νC=O)	12.0	12.0	10.7	10.7
f(νC-C)	4.06	4.06	4.14	4.12
f(νCH₂)	4.75	4.75	4.75	4.75
f(νCH₃)	4.79	4.80	4.78	4.80
f(δCH₂)	0.70	0.70	0.70	0.70
f(δCH₃)	0.53	0.53	0.52	0.52

Units are mdyn $Å^{-1}$ for stretching and mdyn Å rad^{-2} for angle deformations; [a]This work

5. Ultraviolet-visible spectra

The electronic spectra of both R(+) and S(-) forms of camphor were predicted in aqueous solution by using the B3LYP/6-311++G** method and TD-DFT calculations with the Gaussian 09 program [48]. Comparisons between the predicted spectra of R(+) and S(-) forms with the corresponding experimental available from Ref [3] are given in **Figure 8**. A maximum it is observed at 289 nm in the experimental available UV-Vis spectrum of camphor in methanol solution taken form Ref [3] while in the experimental UV-Vis spectrum recorded for camphor in ethanol solution the position of maximun it is

observed at 296 nm [62]. In the predicted UV-Vis spectra for both R(+) and S(-) forms of camphor are observed three bands, two intense at 152 and 169 nm while other two at 190 and a very weak at c.a. 300 nm. Obviously, the predicted bands between 150 and 200 nm are not observed in the experimental spectrum because it was recorded between 200 and 400 nm. The low intensity of band predicted for both forms of camphor at 300 nm can be atributted to the symmetry forbidden n→π* transition in ketones and, hence, camphor has extremely low capacity of UV absorption, as reported by L. Sousa et al. [62]. NBO calculations have predicted for both forms of camphor the σ→σ* transitions with higher intensities (305-302 kJ/mol) while the n→σ* (182-169 kJ/mol) and σ→π* transitions present lower intensities (62-58 kJ/mol). Evidently, both UV-Vis spectra predicted for the R(+) and S(-) forms of camphor can be present in solution, as also suggest the ^{1}H- and ^{13}C-NMR spectra.

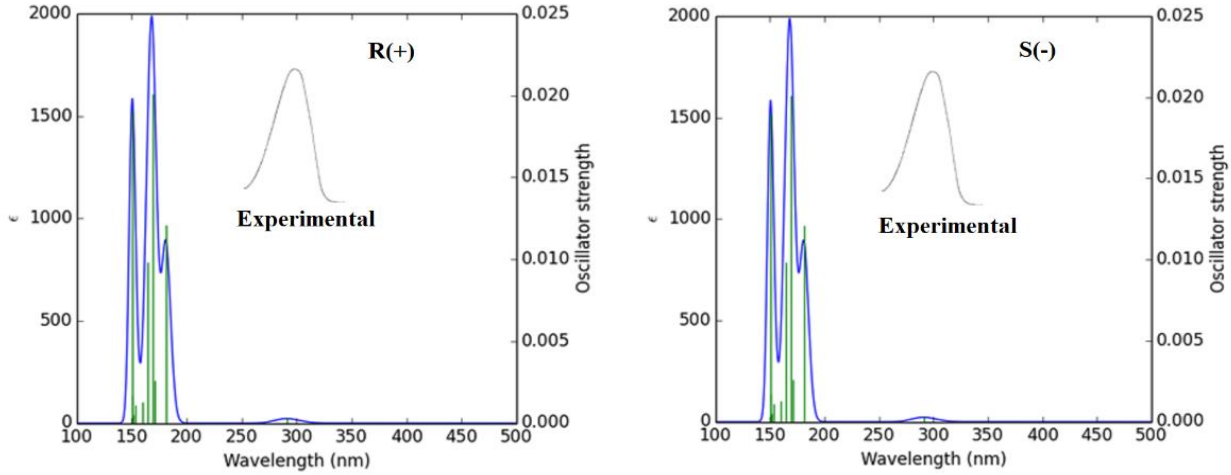

Figure 8. Predicted UV-visible spectra of both R(+) and S(-) forms of camphor in aqueous solution by using the B3LYP/6-311++G** method compared with the corresponding experimental one taken from Ref [3].

6. Electronic circular dichroism (ECD)

The ECD spectra of both R(+) and S(-) forms of camphor were predicted in aqueous solution by using the B3LYP/6-311++G** method and TD-DFT calculations with the Gaussian 09 program [48]. In **Figure 9** can be seen comparisons between the predicted spectra of R(+) and S(-) forms with the corresponding experimental available from Ref [62].

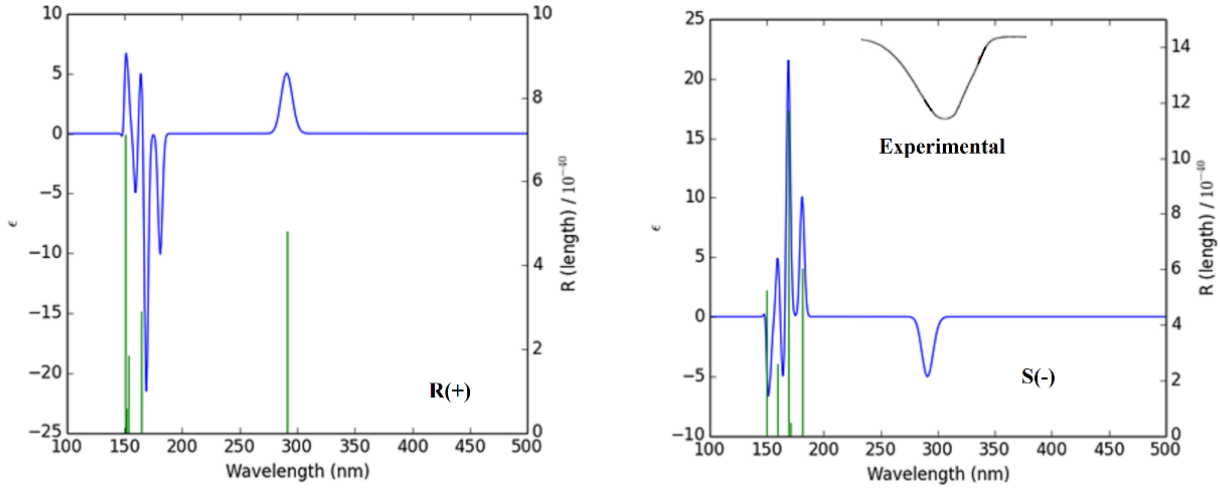

Figure 9. Predicted ECD spectra of both R(+) and S(-) forms of camphor in aqueous solution by using the B3LYP/6-311++G** method compared with the corresponding experimental one for the S(-) form of camphor taken from Ref [62].

The negative band observed in the predicted ECD spectrum of S(-) form is in accordance with that experimental reported for S-camphor at c.a. 300 nm by L. Sousa et al. [62]. The ECD spectrum predicted for the R(+) form of camphor is observed a positive band at 300 nm different from the experimental one recorded for the S(-) form of camphor, as expected. The graphic for the S(-) form shows an ECD spectrum similar to the experimental one (negative value).

Conclusion

In this work, the structures of two enantiomeric *Cis* S(-) and R(+) forms of camphor were theoretically determined by using hybrid B3LYP/6-311++G** calculations in gas phase and aqueous solution. Very good concordances were observed in the geometrical parameters as compared with the corresponding experimental of (+)-3-bromocamphor. The properties in solution and the solvation energies were studied with the SCRF methods together with IEFPCM and universal solvation methods. Differences in solvation energy values of both forms are predicted at the same level of theory having the R(+) form (-39.65 kJ/mol) a higher value than the other one (-37.56 kJ/mol). Probably, the changes of signs predicted in the dihedral C11-C3-C2-C4 angles of both forms in the two media could explain the different solvation energy values and the different positions of H atoms of CH_3 groups in relation to O1 atoms of C8=O1 bonds. Nucleophilic sites are observed on only acceptor H bonds (O1 atoms) in both forms. NBO calculations predict only $\Delta E_{\sigma\rightarrow\sigma^*}$, $\Delta E_{\sigma\rightarrow\pi^*}$ and $\Delta E_{n\rightarrow\sigma^*}$ interactions althougth the expected $\Delta E_{n\rightarrow\pi^*}$ transitions due to ketone groups C=O were no predicted. Gap and electrophilicity index (ω) values of both forms of camphor are close to the value observed in antiviral thymidine. Such observations could be explained by the proximities between the acceptor groups H bonds (C=O) and the CH_3 groups present in both camphor and thymidine species. Reasonable concordances were found among the predicted ^{1}H- and ^{13}C-NMR, UV-visible, ECD, IR and Raman spectra with the corresponding experimental ones. The complete vibrational assignments and scaled force constants for both forms camphor are reported for first time.

Acknowledgements. This work was supported with grants from CIUNT Project Nº 26/D608 (Consejo de Investigaciones, Universidad Nacional de Tucumán).

Supporting Information Available: Tables from S1-S8 and Figures S1-S3.

References

1. C. I. Bliss, A. W. Cressman, B. M. Broadbent, Productivity of the camphor scale and the biology of its egg and crawler stages, *Journal of Agricultural Research*, 50(3) (1935) 243-266
2. F.H. Allen, D. Rogers, X-Ray Studies of Terpenoids. Part llL1 A Redetermination of the Crystal Structure of (+)-3-Bromocamphor: the Absolute Configuration of (+)-Camphor *J. Chem. Soc.* (B) 4, 632-61, (1971) 117079
3. M. Tariq, A.A. Al-Badr, Camphor, AnalyticaI Profiles of Drug Substances, *Academy Press, Inc.* (1984)
4. Helena Dodziuk, Andrzej Ejchart, Oleg Lukin, Vysotsky, M.O. 1H and 13C NMR and Molecular Dynamics Study of Chiral Recognition of Camphor Enantiomers by α-Cyclodextrin, *Org. Chem.* 64 (1999) 1503-1507.
5. C.D. Frizzo, A.C. Santos, N. Paroul, L.A. Serafini, E. Dellacassa, D. Lorenzo, P. Moyna, Essential Oils of Camphor Tree (*Cinnamomum camphora* Nees & Eberm) Cultivated in Southern Brazil, *Braz. arch. biol. technol.* 43(3) (2000) 1-3.

6. Z. Kisiel, O. Desyatnyk, E. Białkowska-Jaworska, L. Pszczółkowski, The structure and electric dipole moment of camphor determined by rotational spectroscopy, *Phys. Chem. Chem. Phys.* 5 (2003) 820-826
7. A.S. Manoguerra, A.R. Erdman, P.M. Wax, L.S. Nelson, E.M. Caravati, D.J. Cobaugh, P.A. Chyka, K.R. Olson, L.L. Booze, A.D. Woolf, D.C. Keyes, G. Christianson, E.J. Scharman, W.G. Troutman, Camphor Poisoning: an Evidence-Based Practice Guideline for Out-of-Hospital Management, *Clinical Toxicology*, 44 (2006) 357–370.
8. C.F. Poe, Studies on the determination of camphor in camphor liniment. IV. The use of antioxidants, Journal of the American Pharmaceutical Association, 25(4) (2006) (279-281).
9. C.F. Poe, Studies on the determination of camphor in camphor liniment. III. Vacuum oven method, Journal of the American Pharmaceutical Association, 21(4) (2006) (337-341).
10. E. Debie, L. Jaspers, P. Bultinck, W. Herrebout, B. Van Der Vekenk, Induced solvent chirality: A VCD study of camphor in CDCl3, *Chemical Physics Letters* 450 (2008) 426–430.
11. P. Zuccarini, Camphor: risks and benefits of a widely used natural product, *J. Appl. Sci.* Environ. *Manage.* 13(2) (2009) 69-74
12. W.C. Evans, Revised with the assistance of Daphne Evans BA MA, Trease and Evans' Pharmacognosy (Sixteenth Edition), Chapter 22 - Volatile oils and resins, (2009) 263-303.
13. I. Duarte, R. Lazzarini, A. Rotter, C. Kobata, Side Effects of Drugs Annual, Chapter 14 - Dermatological drugs, topical agents, and cosmetics, 33 (2011) 333-343.
14. J.R. Schenk, Phytochemistry, allelopathy and the capability attributes of camphor laurel (Cinnamomum camphora (L.) Ness & Eberm.), Southern Cross University, Thesis, ePublications@SCU (2009).
15. D.B.Strader, V.J. Navarro, L.B.Seeff, Chapter 26 - Hepatotoxicity of Herbal Preparations, Zakim and Boyer's Hepatology (Sixth Edition), (2012) 462-475.
16. J.A. Cody, R.K. Boeckman Jr. Reference Module in Chemistry, Molecular Sciences and Chemical Engineering, Comprehensive Chirality, 3.3 Terpene Derived Auxiliaries: Camphor and Pinene Derived Auxiliaries, 3 (20129 42-105.
17. K. Cima, J. Twiss, R. Speich, S.P. McKenna, E. Grünig, C.M. Kähler, N. Ehlken, U. Treder, S.R. Crawford, L.C. Huber, S. Ulrich, The German adaptation of the Cambridge pulmonary hypertension outcome review (CAMPHOR), Cima et al. Health and Quality of Life Outcomes (2012).
18. R. Hamidpour, S. Hadmipour, M. Hamidpour, M. Shahlari, Camphor (*Cinnamomum camphora*), with the history of treating seveartal diseases, *IJCRI* 4(2) (2013) 86–89.
19. W. Chen, I. Vermaak, A. Viljoen, Camphor—A Fumigant during the Black Death and a Coveted Fragrant Wood in Ancient Egypt and Babylon—A Review, *Molecules* 18 (2013) 5434-5454.
20. H.L.Rivera, F.Barrueto, Camphor, Encyclopedia of Toxicology (Third Edition), Reference Module in Biomedical Sciences, (2014) 627-629.
21. R. Tisserand, R. Young, Essential Oil Safety (Second Edition), A Guide for Health Care Professionals, 13 - Essential oil profiles, (2014) 187-482.
22. A.T. Yousefi, S. Bagheri, K. Shinji, J. Rouhi, M.R. Mahmood, S. Ikeda, Fast Synthesis of Multilayer Carbon Nanotubes from Camphor Oil as an Energy Storage Material, Hindawi Publishing Corporation BioMed Research International Volume 2014, Article ID 691537, 6 pages.
23. T. Kotaka, S. Kimura, M. Kashiwayanagi, J.Iwamoto, Camphor Induces Cold and Warm Sensations with Increases in Skin and Muscle Blood Flow in Human, *Biol. Pharm. Bull*. 37(12) (2014) 1913-1918

24. J.T. Fu, L. Tang, W.S. Li, K.Wang, D.M. Cheng, Z.X. Zhang, Fumigant Toxicity and Repellence Activity of Camphor Essential Oil from Cinnamonum camphora Siebold Against Solenopsis invicta Workers (Hymenoptera:Formicidae), *J. Insect Sci*. 15(1) (2015) 129.
25. S. Rahnama-Moghadam, L.D. Hillis, R.A. Lange, Heart and Toxins, Chapter 3 - Environmental Toxins and the Heart, (2015) 75-132.
26. Meyler's Side Effects of Drugs (Sixteenth Edition), The International Encyclopedia of Adverse Drug Reactions and Interactions, (2016) 44.
27. Meyler's Side Effects of Drugs (Sixteenth Edition), The International Encyclopedia of Adverse Drug Reactions and Interactions, Lauraceae, (2016) 484-486.
28. S.C. Sikka, A.R. Bartolome, Bioenvironmental Issues Affecting Men's Reproductive and Sexual Health, Chapter 36 - Perfumery, Essential Oils, and Household Chemicals Affecting Reproductive and Sexual Health, (2018) 557-569.
29. Y. Moayedi, S.A Greenberg, B.A Jenkins, K.L Marshall, L.V Dimitrov4, A.M Nelson, D.M Owens, E.A Lumpkin, Camphor white oil induces tumor regression through cytotoxic T cell-dependent mechanisms, *Molecular Carcinogenesis* 58(5) (2019) 722-734. https://doi.org/10.1002/mc.22965.
30. R.J.G. Loffler, M.M. Hanczyc, J. Gorecki, A hybrid camphor–camphene wax material for studies on self-propelled motion, Phys.Chem. *Chem.Phys*. 21 (2019) 2485.
31. R. Hamidpour, S. Hamidpour, M. Hamidpour, R. Hamidpour, The Effect of Camphor Discovery for Treating Asthma, *Adv Bioeng Biomed Sci Res*, 2019, 2(1) 1-4.
32. Mishra VN, Camphor Addiction: A Prospective Study of Camphorated Oil Use & its Outcome over the Period of 10 Years in Tertiary Care Centre, *Clin Neurol*. 1(1) (2020) 1007.
33. J. Shen, A preliminary study on the relation between camphor wood volatile matters and corrosion of museum metallic objects, *2020 IOP Conf. Ser.: Earth Environ. Sci.* 467 012147. doi:10.1088/1755-1315/467/1/012147
34. P. Pulay, G. Fogarasi, G. Pongor, J.E. Boggs, A. Vargha, Combination of theoretical ab initio and experimental information to obtain reliable harmonic force constants. Scaled quantum mechanical (QM) force fields for glyoxal, acrolein, butadiene, formaldehyde, and ethylene. *J. Am. Chem. Soc*., 1983, 105, 7073.
35. G. Rauhut, P. Pulay, Transferable Scaling Factors for Density Functional Derived Vibrational Force Fields. *J. Phys. Chem.* 1995, 99, 3093-3100,
36. T. Sundius, Scaling of ab-initio force fields by MOLVIB. *Vib. Spectrosc.* 2002, 29, 89-95.
37. A.D. Becke, Density-functional exchange-energy approximation with correct asymptotic behavior, *Phys. Rev.* 1988, A38, 3098-3100.
38. C. Lee, W. Yang, R.G. Parr, Development of the Colle-Salvetti correlation-energy formula into a functional of the electron density. *Phys. Rev.* 1988, B37, 785-789.
39. S. Miertus, E. Scrocco, J. Tomasi, Electrostatic interaction of a solute with a continuum. *Chem. Phys.* 55 (1981) 117–129.
40. J. Tomasi, J. Persico, Molecular Interactions in Solution: An Overview of Methods Based on Continous Distributions of the Solvent, *Chem. Rev.* 94 (1994) 2027-2094.
41. A.V. Marenich, C.J. Cramer, D.G. Truhlar, Universal solvation model based on solute electron density and a continuum model of the solvent defined by the bulk dielectric constant and atomic surface tensions, *J. Phys. Chem*. B113 (2009) 6378-6396.
42. Parr, R.G., Pearson, R.G. Absolute hardness: companion parameter to absolute electronegativity, *J. Am. Chem. Soc*. 105 (1983) 7512-7516.

43. R.A. Rudyk, M.A. Checa, C.A.N. Catalán, S.A. Brandán, Structural, FT-IR, FT-Raman and ECD studies on the free base, cationic and hydrobromide species of scopolamine alkaloid, *J Mol. Struct*. 1180 (2019) 603-617.
44. M.E. Manzur, S.A. Brandán, S(-) and R(+) Species Derived from Antihistaminic Promethazine Agent: Structural and Vibrational Studies, *Heliyon* 5 (2019) e02322.
45. D. Romani, M.J. Márquez, M.B. Márquez, S.A. Brandán, Structural, topological and vibrational properties of an isothiazole derivatives series with antiviral activities, *J. Mol. Struct*. 1100 (2015) 279-289.
46. Experimental available ATR, IR and Raman spectra of camphor from: https://spectrabase.com/spectrum/
47. A.B. Nielsen, A.J. Holder, Gauss View 5.0, User's Reference, GAUSSIAN Inc., Pittsburgh, PA, 2008.
48. M.J. Frisch, G. W. Trucks, H.B. Schlegel, G.E. Scuseria, M.A. Robb, J.R. Cheeseman, G. Scalmani, V. Barone, B. Mennucci, G.A. Petersson, H. Nakatsuji, M. Caricato, X. Li, H.P. Hratchian, A.F. Izmaylov, J. Bloino, G. Zheng, J.L. Sonnenberg, M. Hada, M. Ehara, K. Toyota, R. Fukuda, J. Hasegawa, M. Ishida, T. Nakajima, Y. Honda, O. Kitao, H. Nakai, T. Vreven, J.A. Montgomery, Jr, J.E. Peralta, F. Ogliaro, M. Bearpark, J.J. Heyd, E. Brothers, K. N. Kudin, V.N. Staroverov, R. Kobayashi, J. Normand, K. Raghavachari, A. Rendell, J.C. Burant, S.S. Iyengar, J. Tomasi, M. Cossi, N. Rega, J.M. Millam, M. Klene, J.E. Knox, J.B. Cross, V. Bakken, C. Adamo, J. Jaramillo, R. Gomperts, R.E. Stratmann, O. Yazyev, A.J. Austin, R. Cammi, C. Pomelli, J.W. Ochterski, R.L. Martin, K. Morokuma, V.G. Zakrzewski, G.A. Voth, P. Salvador, J.J. Dannenberg, S. Dapprich, A.D. Daniels, O. Farkas, J.B. Foresman, J.V. Ortiz, J. Cioslowski, and D.J. Fox, Gaussian, Inc., Wallingford CT, 2009.
49. P. Ugliengo, MOLDRAW Program, University of Torino, Dipartimento Chimica IFM, Torino, Italy, 1998.
50. E.D. Glendening, J.K. Badenhoop, A. D. Reed, J. E. Carpenter, F. Weinhold, NBO 3.1; Theoretical Chemistry Institute, University of Wisconsin; Madison, WI, (1996).
51. R.F.W. Bader, Atoms in Molecules, A Quantum Theory, Oxford University Press, Oxford, (1990), ISBN: 0198558651.
52. F. Biegler-Köning, J. Schönbohm, D. Bayles. AIM2000; A Program to Analyze and Visualize Atoms in Molecules, *J. Comput. Chem.* 22 (2001) 545.
53. B.H. Besler, K.M. Merz Jr, P.A. Kollman, Atomic charges derived from semiempirical methods, *J. Comp. Chem.* 11(1990) 431-439.
54. R. Ditchfield, Self-consistent perturbation theory of diamagnetism. I. A gage-invariant LCAO (linear combination of atomic orbitals) method for NMR chemical shifts, *Mol Phys*. 27 (1974) 714–722.
55. G. Keresztury, S. Holly, G. Besenyei, J. Varga, A.Y. Wang, J.R. Durig. Vibrational spectra of monothiocarbamates-II. IR and Raman spectra, vibrational assignment, conformational analysis and *ab initio* calculations of *S*-methyl-*N*,*N*-dimethylthiocarbamate, *Spectrochim. Acta*, 49A (1993) 2007-2026.
56. D. Michalska, R. Wysokinski, The prediction of Raman spectra of platinum(II) anticancer drugs by density functional theory, *Chemical Physics Letters*, (2005), 403, 211-217.
57. M.B. Márquez, S.A. Brandán, A structural and vibrational investigation on the antiviral deoxyribonucleoside thymidine agent in gas and aqueous solution phases, *International J. of Quantum Chem.* 114 (3) (2014) 209-221.

58. E. Romano, N. Issaoui, M.E. Manzur, S.A. Brandán, Structural, Vibrational and Molecular docking studies of Potential Antiviral to COVID-19 Chloroquine combining DFT calculations with SQMFF methodology, submitted to Heliyon (2020).
59. M. Minteguiaga, E. Dellacassa, M.A. Iramain, C.A.N. Catalán, S.A. Brandán. Synthesis, spectroscopic characterization and structural study of 2-isopropenyl-3-methylphenol, carquejiphenol, a carquejol derivative with potential medicinal use. *J Mol. Struct*. 1165 (2018) 332-343.
60. M. Minteguiaga, E. Dellacassa, M.A. Iramain, C.A.N. Catalán, S.A. Brandán, A structural and spectroscopic study on carquejol, a relevant constituent of the medicinal plant Baccharis trimera (Less.) DC. (Asteraceae), *J Mol. Struct.* 1150 (2017) 8-20.
61. M. Minteguiaga, E. Dellacassa, M.A. Iramain, C.A.N. Catalán, S.A. Brandán, FT-IR, FT-Raman, UV-Vis, NMR and structural studies of Carquejyl Acetate, a component of the essential oil from *Baccharis trimera* (Less.) DC. (Asteraceae). *J Mol. Struct.* 1177 (2019) 499-510.
62. Iran da L. Sousa, Gabriel Heerdt, Valdecir F. Ximenes, Aguinaldo R. de Souza, Nelson H. Morgon TD-DFT Analysis of the Dissymmetry Factor in Camphor, *J. Braz. Chem. Soc.*, 31 (2020) 613-618. http://dx.doi.org/10.21577/0103-5053.20190226

(2020) ; http://www.jmaterenvironsci.com